Superlattices and Microstructures, Vol. 20, No. 4, 1996

Practical issues in the realization of quantum-dot cellular automata

Gary H. Bernstein, Greg Bazan, Minhan Chen, Craig S. Lent,
James L. Merz, Alexei O. Orlov, Wolfgang Porod,
Greg L. Snider, P. Douglas Tougaw
Dept. of Electrical Engineering, University of Notre Dame, Notre Dame, IN 46556, U.S.A.

(Received 20 May 1996)

Several practical issues in the development and operation of quantum-dot cellular automata (QCA) cells and systems are discussed. The need for adiabatic clocking of QCA systems and modeling of electrostatic confinement of quantum dots are presented. Experimental data on dot coupling and applications to QCA detectors in a 2-dimensional electron gas (2DEG) are presented. We report a charge detection scheme where we observe strong modulation in the detector signal, in addition to the detector exhibiting minimal effect on the dot being measured. With this investigation, we demonstrate these two key components required for QCA in AlGaAs/GaAs materials, namely dot coupling and charge-state detection.

1. Introduction

Quantum cellular automata (QCA) has been proposed [1, 2] as a new technique for performing computation through the use of quantum dots. The basic principle is shown schematically in Fig. 1A. A QCA cell consists of quantum dots arranged such that, e.g. four sites may be occupied by two electrons with semitransparent barriers connecting the dots in some configuration so that, through tunneling, electrons may arrange themselves in their energetically lowest positions. As shown in the figure, the lowest energy state of the electrons places them at corners of the cells aligned along either diagonal, the polarization of which can correspond to either a logic '1' or '0'.

Two cells may be placed adjacent to each other such that they interact only Coulombically, with no tunneling between cells allowed, as shown in the inset of Fig. 1B. The polarization of a cell due to that of its neighbors is very high, such that slight polarization of one cell strongly forces the polarization of its neighbors. Systems designed by Lent *et al*. [3] and Fountain [4] demonstrate that extremely complex digital logic systems can be built up from basic building blocks consisting of 'wires' (chains of cells), invertors, AND gates, OR gates, and majority logic cells. For example, a full adder circuit with a dot size of 10 nm would fit inside an area of about 1 square micron [3]. It is important to note that the design of 'crossover' configurations allows the entire system to exist in a plane, with no out-of-plane interconnects required.

2. Switching behavior of QCA systems

QCA arrays may be switched abruptly, in which case the system is placed in an excited state by the rapid

0749–6036/96/080447 + 13 $25.00/0

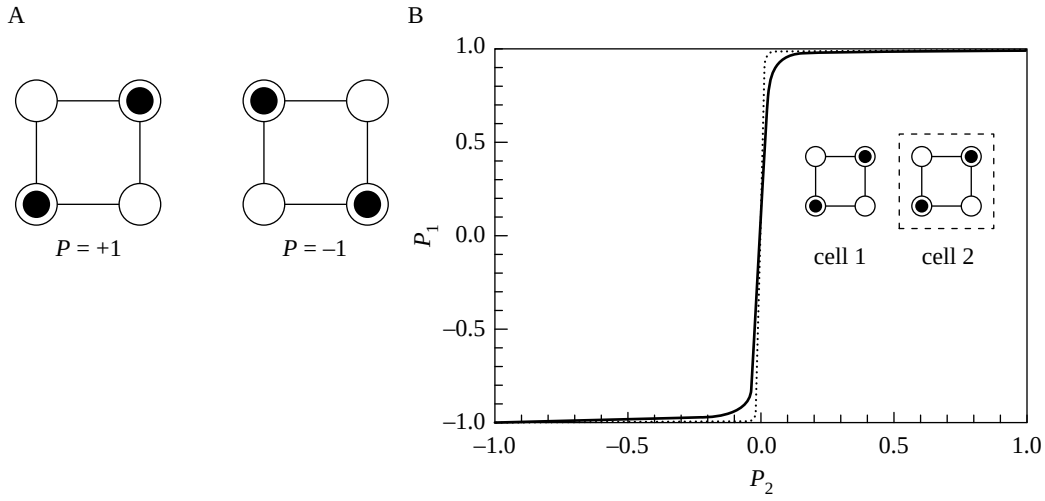

Fig. 1. Quantum-dot cellular automata. A, Schematic of the basic four-site cell. Coulombic repulsion causes the electrons to occupy antipodal sites within the cell. Each configuration can be assigned a digital logic value. B, The cell–cell response. The polarization of cell 2 is fixed and its Coulombic effect on that of cell 1 is measured. The nonlinearity and bistable saturation of this response serves the same role as gain in a conventional digital circuit.

change of a driver cell, and decays through inelastic processes to its ground state. The resulting configuration of the cells is the outcome of a single calculation. It is also possible to switch QCA devices in such a way that the array remains in its instantaneous ground state at all times. The adiabatic theorem guarantees that this is possible if the switching time is slow compared to the time associated with transitions to the first excited state of the array. As shown in Fig. 2, the first step in adiabatic switching is to lower the intra-dot barriers within each cell, reducing the electron localization imposed by high barriers. Barriers between cells remain high. The driver cell polarization is then switched adiabatically, followed by adiabatically re-asserting the barriers, which returns the localization of the electrons and the polarization of the cell.

A study of the allowable speed of such switching has shown that the non-adiabatic error, which is due to switching the devices too quickly to be strictly adiabatic, decreases exponentially with the time during which the devices are switched. This exponential decrease is shown in Fig. 3 for a simple one-cell majority logic gate and a larger five-cell extended majority logic gate. In spite of the fact that the five-cell device requires more time than the single-cell device to switch with the same level of accuracy, both errors decrease exponentially with switching time. Preliminary results on the scaling of switching time with the number of cells in an array have shown switching time increases, at worst, in an approximately linear relationship with the number of cells in an array. Adiabatic switching has the significant advantage that it provides a means of maintaining clocked control over the calculation and eliminates dependence on inelastic processes in accomplishing device switching.

3. Basic elements of QCA systems

The notion that controlled use of single electrons has progressed beyond basic physics is evident from proposals of, for example, circuits and systems based on single electron tunneling [5–7]. Interest in these systems is focusing less on the study of basic physical phenomena, and increasingly on how to assemble building blocks in the design of more complex systems for the attainment of truly revolutionary applications. It is relevant, then, to discuss what are the important building blocks for the creation of QCAs.

The basic elements of QCA require (1) that the appropriate number of (extra) electrons be induced in each

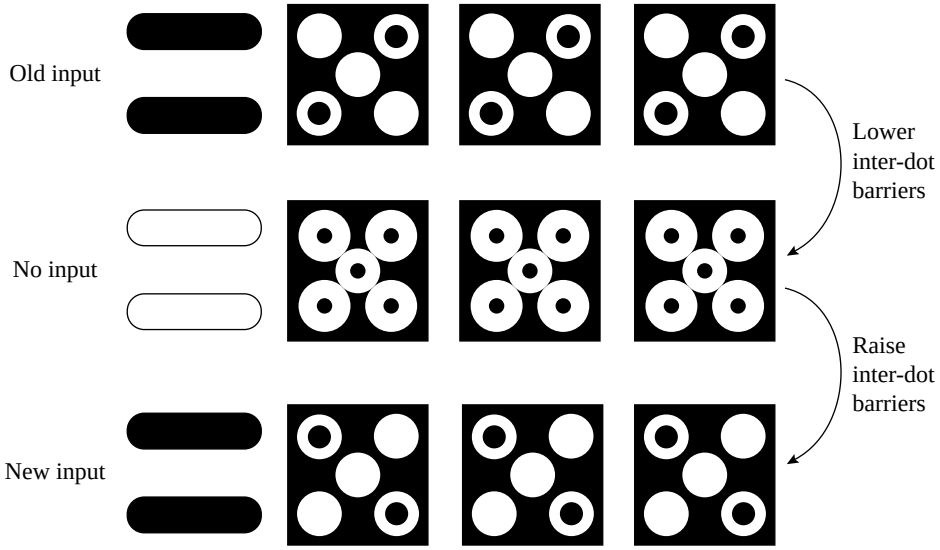

Fig. 2. A schematic representation of the adiabatic switching of an array of QCA cells. The intra-dot barriers are adiabatically lowered, decreasing the localization of the electrons within each cell. The old input is removed, and a new input is applied, followed by a re-application of the intra-dot barriers. This causes the cells to exhibit the ground state corresponding to the new input.

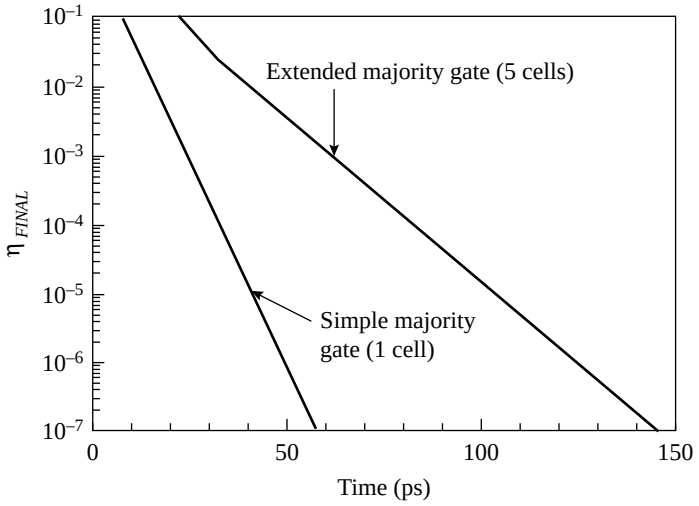

Fig. 3. The non-adiabatic error introduced by switching a QCA array can be measured by the total projection of the cell state on all non-ground state basis vectors after switching is complete. This non-adiabatic error decreases exponentially with the amount of time allowed for switching the device. This figure shows the exponential decrease for two systems—a simple one-cell majority logic gate and a more complicated five-cell extended majority logic gate.

cell, (2) that dots be sufficiently close to allow inter-dot tunneling, (3) that adjacent cells be close enough to permit Coulomb coupling, and (4) that the cell polarization state be detected. Although one can envisage QCA behavior in such varied systems as metal tunnel junctions [8, 9], Si inversion layers, self-assembled quantum dots [10], nanomagnet arrays, vertical quantum dots, or even arrays of individual molecules, we have chosen to do our initial studies in the well-characterized AlGaAs/GaAs system, which currently offers

a large array of useful building blocks. Demonstrations of Coulomb blockade and single electron tunneling through quantum dots for charge entrapment, single electron transistors for control of dot occupancy, and single-electron electrometers [11–13] for charge detection are all available to the design engineers of future single-electronic applications.

4. Modeling for QCAs

For the calculations discussed so far, modeling behavior of arrays of quantum-dot cells, it is appropriate to use an extended Hubbard-type Hamiltonian and describe the individual dots simply as sites. We now turn to the issue of designing the optimal gate patterns to realize these cells in semiconductor systems. For that, one must employ realistic models of the detailed semiconductor-gate geometry.

In order to design optimal cells, it is important that potential profiles and electron density be calculated through the accurate solution of Poisson's equation. To this end, we have performed numerical simulations for the design of quantum dot structures in the few-electron regime, both in the GaAs/AlGaAs and Si/SiO_2 material systems. The confining potential is obtained from the Poisson equation within a Thomas–Fermi charge model. The electronic states in the quantum dot are then obtained from solutions of the axisymmetric Schrödinger equation. Our model takes into account the effect of surface states by viewing the exposed surface as the interface between the semiconductor and air (or vacuum). This is particularly important for modeling the III-V material system, where surface states have to be taken into account. We explore various gate configurations and biasing modes. Our simulations show that the number of electrons can be effectively controlled in the few-electron regime with combined enhancement and depletion gates.

The goal of this modeling is to numerically investigate the feasibility of realizing gate-controlled quantum dots in the few-electron regime for QCA applications. In order to achieve a crisp confining potential, minimization of the effects of fringing fields will be focused on, by bringing the electrons as close as possible to the top surface. This design strategy of 'trading mobility versus gate control' by utilizing near-surface 2DEGs has been pioneered by Snider, Hu and co-workers [14, 15]. However, the resultant proximity of the quantum dot to the surface raises the question of the effect of the exposed surface on the quantum confinement. In our modeling, we explicitly include the influence of surface states which are occupied, in a self-consistent fashion, according to the local electrostatic potential [16]. Our modeling has shown that the simple geometry of a conventional metal electrode used for electrostatic confinement does not provide sufficient gate control for QCA applications, even for extremely shallow 2DEGs. We have therefore explored the use of dual gates which allows one to achieve superior control of the confining potential [17].

We will now demonstrate that a combination of enhancement and depletion gates, as shown in the inset of Fig. 4A, provides effective control of the threshold voltage. The main idea is to negatively bias the outer gates (gate 2) such that the electron density is depleted or near depletion; a positive bias on the inner gate (gate 1) is then utilized to induce the dot and to control its occupation.

Figure 4A shows an example of the size and occupation of quantum dots for combined enhancement/depletion mode biasing on an AlGaAs/GaAs 2DEG. The *n*-type sheet doping concentration for the delta-doped AlGaAs layer is assumed to be 3×10^{12} cm^{-2}. In this example, we have chosen a radius of $r = 6$ nm for the center enhancement gate, and a radius of $r_{G2} = 50$ nm for the surrounding depletion gate. The radius of quantum dots, r_{dot}, induced by three different voltages on the depletion gate, V_{G2}, is plotted as a function of the enhancement gate bias voltage, V_{G1}. Figure 4B shows the corresponding number of electrons in each dot (note that fractional dot occupancies are possible because of the semi-classical model used).

We see that variations of the depletion-gate bias of 10 mV will result in threshold-voltage variations of as much as 80 mV. This biasing mode appears to be an effective way of controlling the quantum-dot threshold voltage in the few-electron regime.

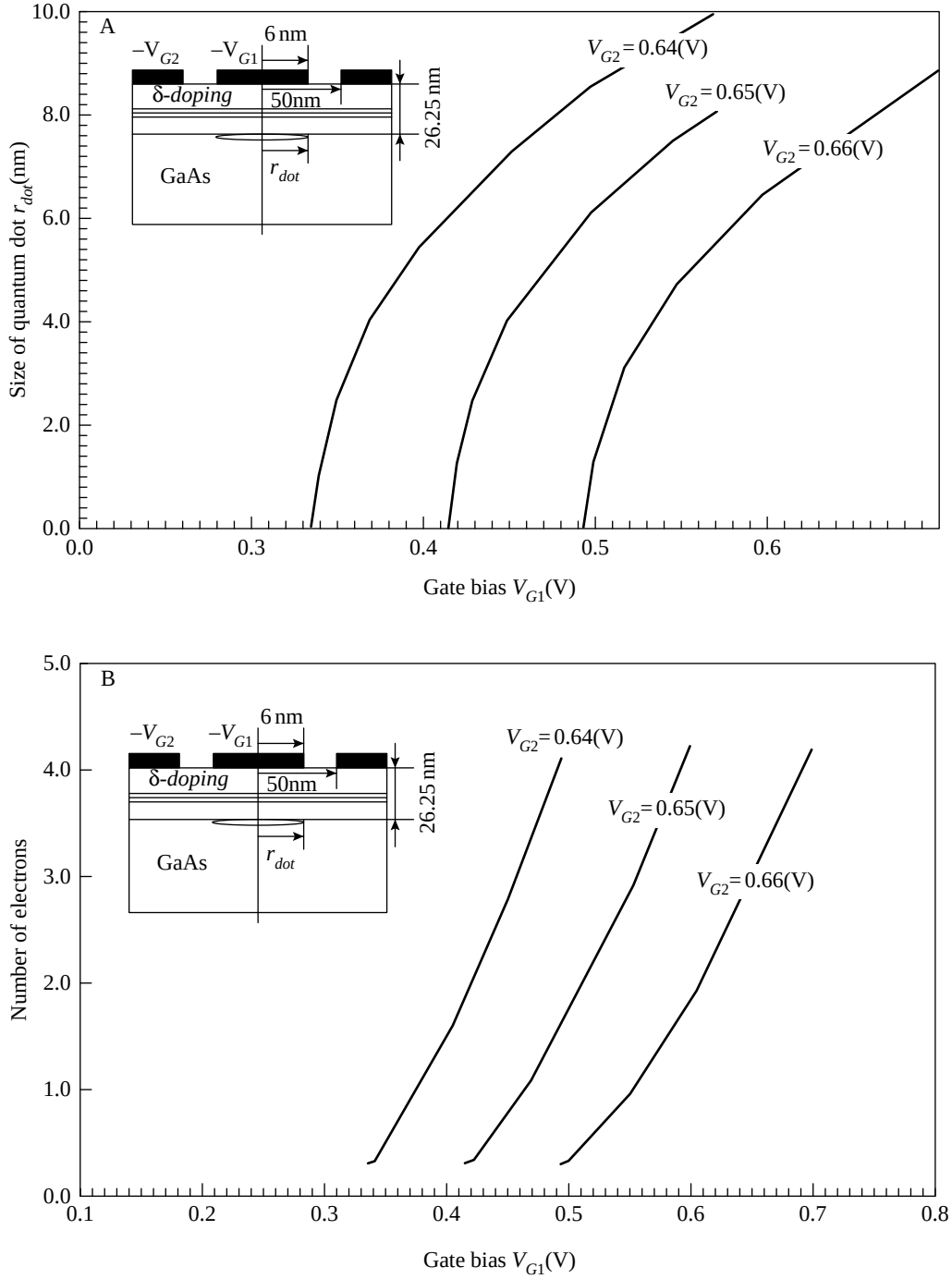

Fig. 4. Size and occupation of quantum dots for combined enhancement/depletion mode biasing. The gate dimensions are indicated in the insets. A, Radius of quantum dots, r_{dot}, induced by three different voltages on the depletion gate, V_{G2}, as a function of the enhancement gate bias voltage, V_{G1}. B, Corresponding number of electrons in each dot.

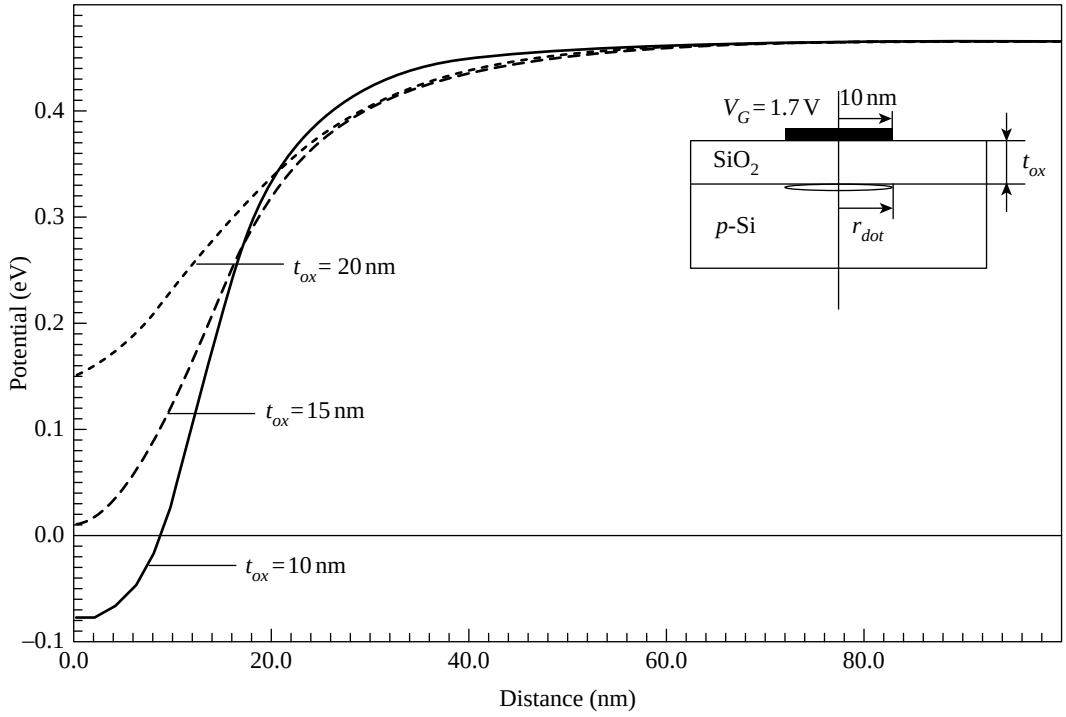

Fig. 5. Quantum dot potential profile along the Si/SiO_2 interface for various oxide thicknesses.

We have also performed numerical simulations for the design of gated few-electron quantum dot structures in the Si/SiO_2 material system. The motivation for this work is to investigate the feasibility of transferring the emerging technology of quantum dot fabrication from the III-V material system, where it was pioneered over the past few years, to the technologically more important Si/SiO_2 structures. Silicon appears to be a promising candidate due to the excellent insulating behavior of thin Si/SiO_2 films which yields the required crisp gate-control of the potential in the plane of the 2DEG at the Si/SiO_2 interface. Another advantage of silicon for quantum dot applications appears to be the higher effective mass, as compared to the III-V materials, which reduces the sensitivity of the energy levels to size fluctuations.

Quantum dots may be realized by applying a positive bias to a metallic gate on the surface, as schematically shown in the inset to Fig. 5. The positive voltage induces an inversion layer underneath the biased gate, which may lead to the formation of an 'electron droplet' at the silicon/oxide interface, i.e. a quantum dot. Figure 5 shows, for an applied gate bias of 1.7 V, the corresponding potential variations along the Si/SiO_2 interface; the Fermi energy is taken as the zero of energy and indicated by the thin horizontal line. An electronic system is induced when the silicon conduction band edge at the oxide interface, indicated by the solid line, dips below the Fermi level. We see that the formation of a quantum dot critically depends upon the thickness of the oxide layer. Our modeling shows that for a 10 nm gate radius, an oxide thickness around (or below) 10 nm is required.

Figure 6A shows, for various oxide thicknesses, the radius of a bias-induced quantum dot, as schematically shown in the inset. The positive bias is applied to a circular gate with 10 nm radius. Figure 6B presents the corresponding number of electrons in the quantum dot, which is obtained by integrating the electron density over the inversion region. The data shows that it should be feasible to create electronic systems with

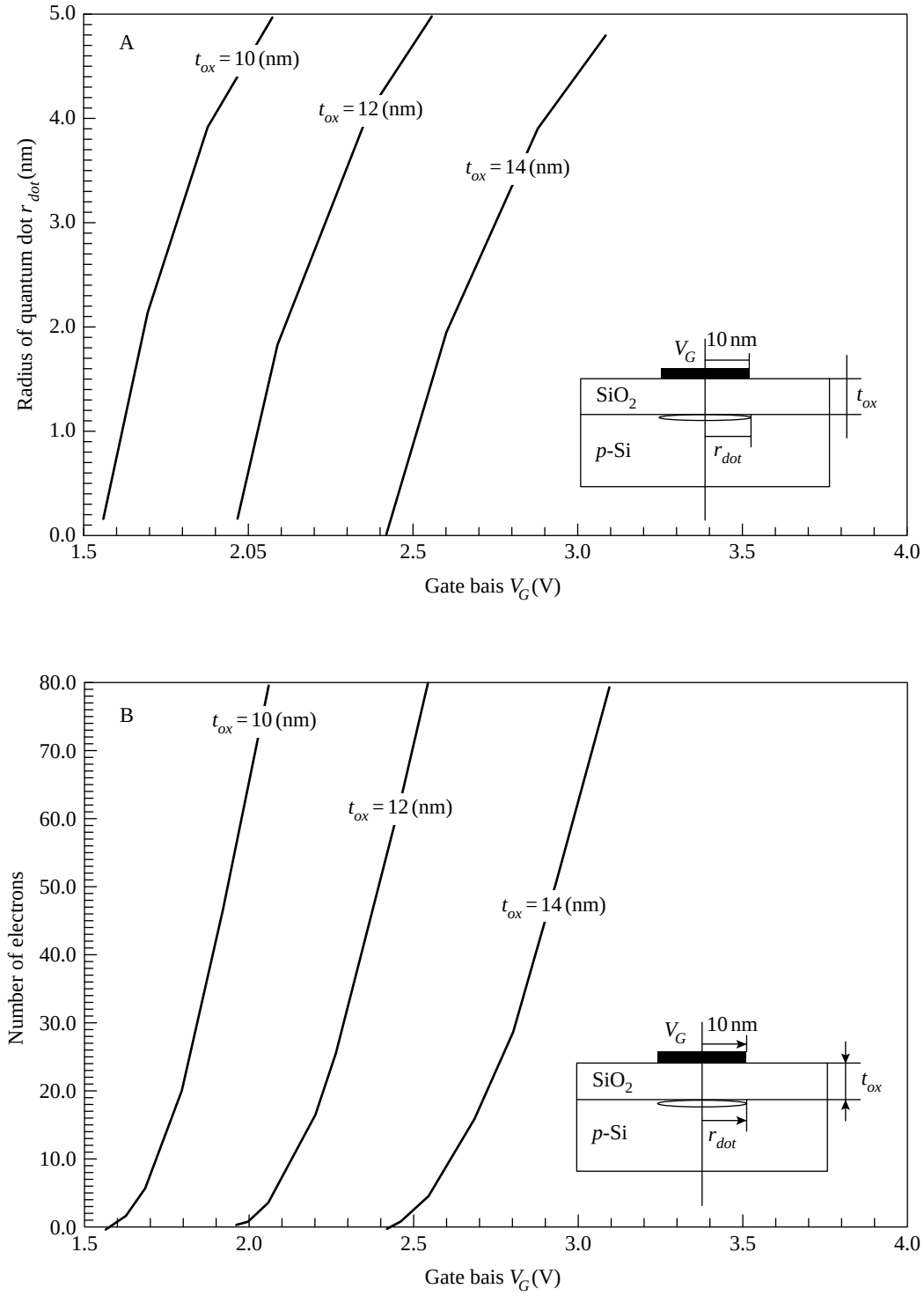

Fig. 6. Gate-induced quantum dot for various oxide thicknesses; shown are, as a function of gate bias, (A) the dot radius, and (B) the number of electrons occupying the dot.

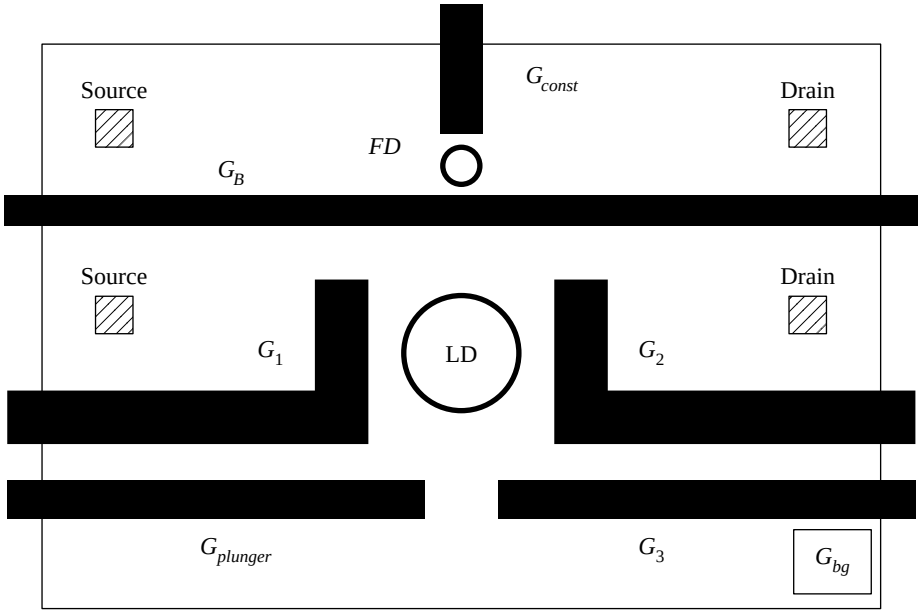

Fig. 7. Schematic diagram of gates and dots used in charge coupling and electrometer experiments.

dimensions on the order of 10 nanometers, and that it should be possible to control the electron occupancy in the few-electron regime.

5. Coupled dot experiments

Dot coupling is the most critical phenomenon required of QCAs, affecting intracellular and intercellular responses to inputs, and providing for an efficient method of charge detection, as we will demonstrate below. Our coupled dot experiments were performed on 2DEG material consisting of a 15 nm undoped AlGaAs spacer layer, a 30 nm n^+-AlGaAs Si-doped donor layer, and a 20 nm n^+-GaAs cap layer, resulting in 2DEG depth of 65 nm. The 2DEG carrier concentration and mobility at 4.2 K were 3×10^{11} cm^{-2} and 4.5×10^5 cm^2 V^{-1} s^{-1}, respectively. Ohmic contacts were formed from AuGeNi, and gates were defined by electron beam lithography (EBL). The cap layer was etched to minimize leakage current. The AuPd gate pattern was produced by EBL, thermal evaporation, and lift-off.

The gate pattern shown in Fig. 7 forms a 1D constriction adjacent to a lithographically defined dot. The lithographic dot (LD) has a total area of 490 $\times$ 360 nm^2 when negative gate voltages are applied to corresponding gates G_B, G_1, G_2, G_3, $G_{plunger}$. The constrictions between G_b–G_1 and G_b–G_2 form tunneling barriers through which the dot is weakly coupled to the source and drain. A back-gate contact was fabricated for further control of carrier concentration. All experiments were performed in a ^{3}He system with base temperature of 300 mK. Conductance was measured using standard lock-in techniques with a 10 μV excitation voltage at 10–20 Hz. The constriction and dot circuits were measured with separate lock-in amplifiers at different frequencies.

The population of the lithographic dot can be changed by varying any of the top or back gate potentials. At low temperatures ($<$ 0.6 K) Coulomb blockade oscillations (CBO) with a distinct frequency were observed as a function of the plunger gate voltage, $V_{plunger}$ (Fig. 8A).

For certain settings of $V_{constriction}$, we also observed conductance resonances as a function of $V_{plunger}$ in

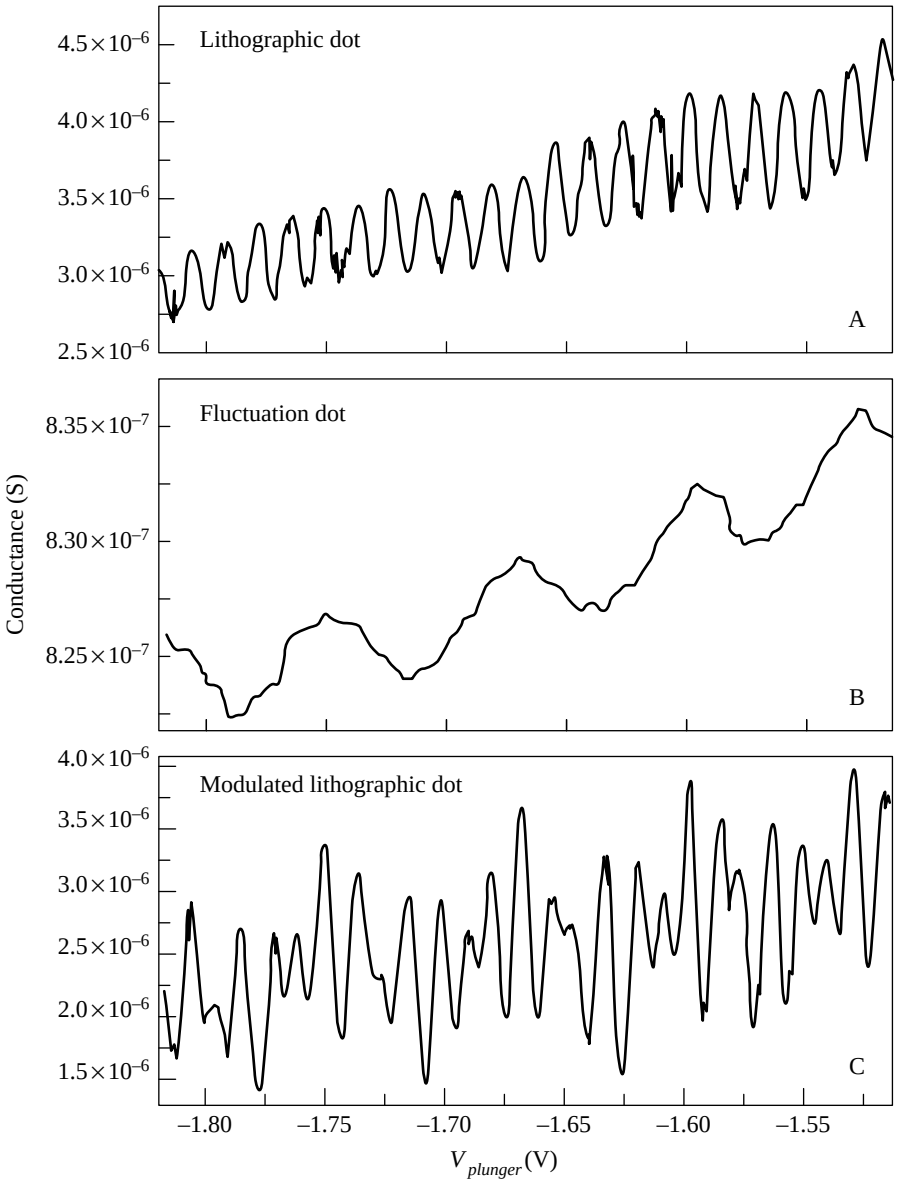

Fig. 8. Single electron tunneling conductance oscillations as a function of plunger gate voltage for (A) lithographic dot in the absence of fluctuation dot charging, (B) fluctuation dot, and (C) lithographic dot in the presence of fluctuation dot charging.

the narrow constriction adjacent to LD, shown in Fig. 8B. We believe these conductance oscillations were due to the depopulation of charge trapped by a random fluctuation potential in the narrow constriction. Such 'fluctuation dots' (FD) have been studied previously in several different systems [18–21], and conductance oscillations were interpreted in terms of Coulomb blockade transport through a quantum dot formed by fluctuation potentials. A post-measurement examination by field emission scanning electron microscopy revealed small ($\sim$ 20 nm) islands of n^+ GaAs on the surface, which may be the source of the fluctuation potential seen by electrons at the AlGaAs/GaAs interface.

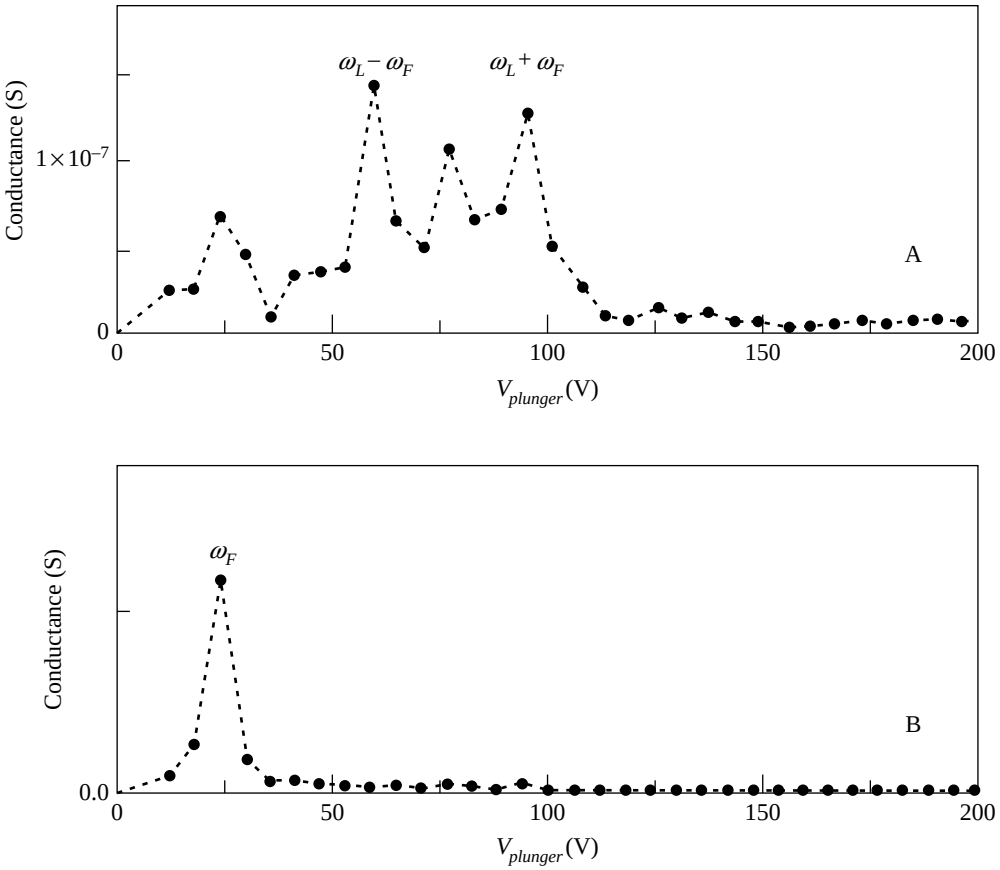

Fig. 9. Fourier transform spectra of conductance oscillations for (A) lithographic dot in the presence of fluctuation dot charging and (B) fluctuation dot charging.

The resistance of the barrier between the 1D constriction and the dot was determined to be greater than 100 GΩ, guaranteeing that the dot in the 1D constriction and the lithographic dot were not directly coupled. With proper bias settings, LD CBOs changed dramatically when FD CBOs were measured, as shown in Fig. 8C, with the Fourier transform (FFT) spectrum shown in Fig. 9A. The presence of $\omega_L + \omega_F$ and $\omega_L - \omega_F$ components are clearly seen. Almost no trace of the LD signal is seen in the FD FFT spectrum (Fig. 9B). In addition, sweeping the back-gate contact resulted in similar behavior of the two dots. The current through LD exhibited periodic oscillations as a function of external charge when no other charge was present. The periodicity of the LD oscillations was modified by the charging of the FD.

Our system is comparable to the metal tunnel junction system discussed by Lafarge *et al*. [22], with an equivalent circuit shown in Fig. 10. The plunger affects the population of both LD and FD. As the population of FD changes, it in turn modulates the population of LD. Assuming FD is smaller than LD, as expected from lithographic constraints, the behavior can be explained in terms of the relative charging energies of the dots. Since FD possesses less total capacitance, its charging energy is larger than that of LD, and its conductance oscillations occur with a larger period in $V_{plunger}$. Although the coupling capacitor C_c connects the dots, a change in the occupancy of FD by one electron results in a larger potential shift than for a similar change in occupancy of LD. Therefore, feedback of LD, acting now as an electrometer sensing the charge of FD, is

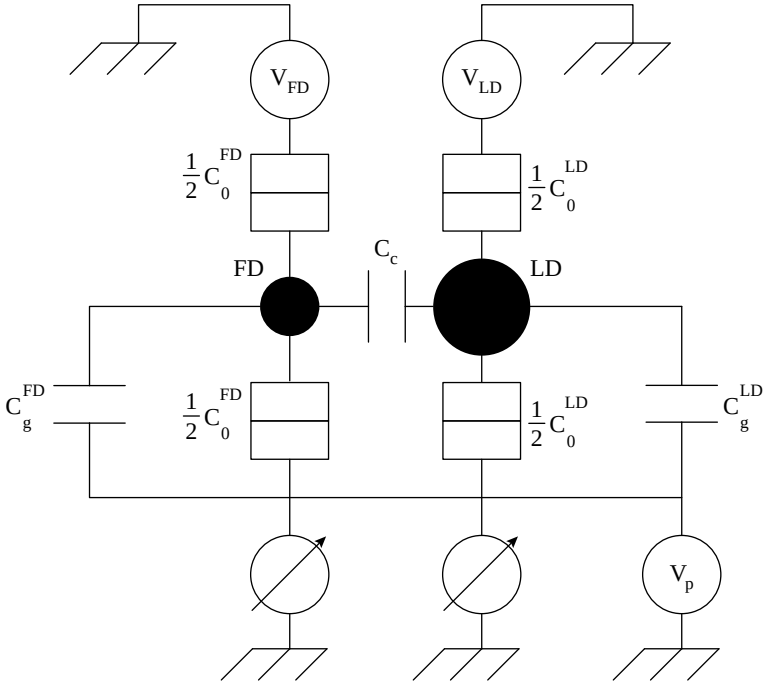

Fig. 10. Equivalent circuit of the lithographic and fluctuation dot configuration.

minimized since FD requires a larger contribution to its potential by LD in order to change its charge state. However, because LD is relatively large, its charging energy is small and changes in the potential of FD create a noticeable effect on its charge state.

Figure 11 shows the results of our model using the equivalent circuit of Fig. 10, and our experimentally-derived capacitance values. Parts (A) and (B) show LD junction charge and dot population as functions of $V_{plunger}$, with and without the presence of FD. Figure 11(C) and (D) show the same information for FD. It is clear that the additional potential from FD causes the positions of the population transitions of LD to shift relative to their positions without FD. Since the conductance peaks occur at population transitions, these shifts produce a clear modulation in the period of the conductance oscillations.

6. Summary and conclusions

We have discussed several practical issues in the study of theoretical and experimental QCA behavior. We have shown that adiabatic switching of QCAs is preferable to abrupt switching, and that double-gated structures are preferable to single-gated ones, resulting in very good control of dot size and occupancy. We have also demonstrated charge coupling between two quantum dots, and their behavior as a sensitive electrometer for the detection of single electron charging. The data was easily interpreted in terms of an equivalent circuit with a coupling capacitor between the two dots. These data indicate that a useful way of detecting the charge state of a QCA cell will be through the use of larger quantum dots as detectors of smaller dots. We have demonstrated repeatable lithographic dots of various sizes, and designed and fabricated six-dot cells guided by the results discussed here. The six-dot design incorporates four dots connected by tunnel junctions, forming the QCA cell, and two adjacent dots to be used as detectors, according to the results described in this paper. When an electron shifts between dots it is expected that the behavior of the non-invasive probe dots will be

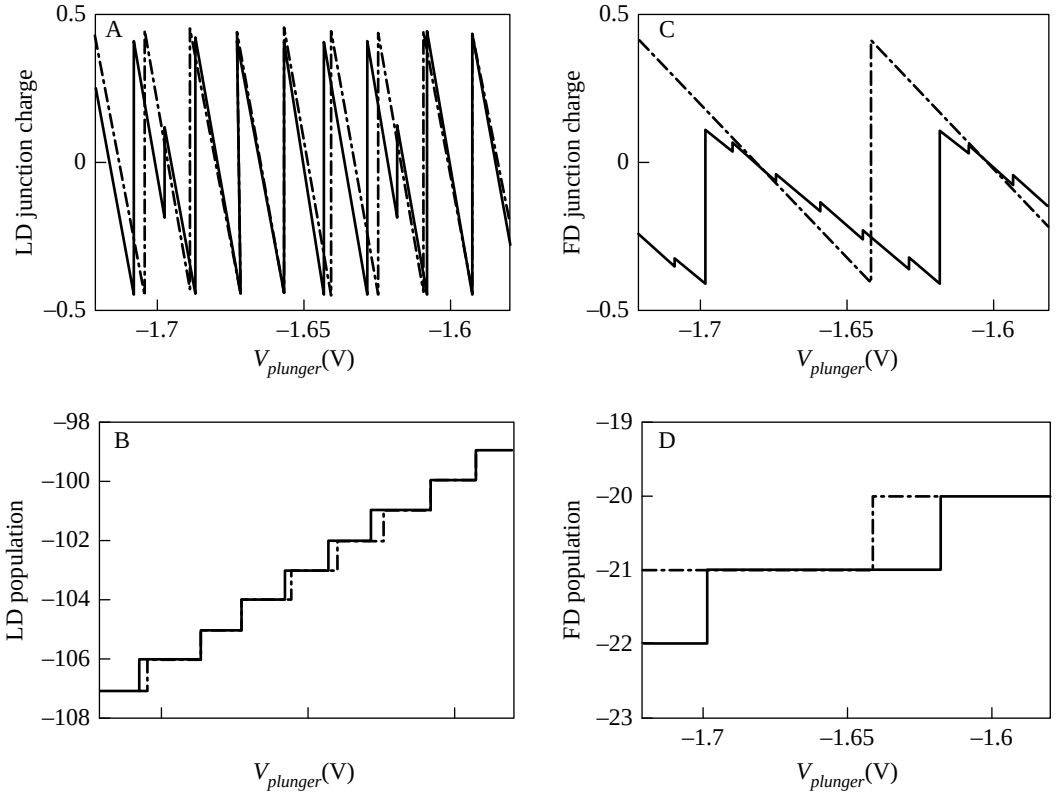

Fig. 11. Numerical simulation of the $V_{plunger}$ dependence, with dot coupling (——) and without dot coupling (— · —), of (A) LD junction charge, (B) LD electron population, (C) FD junction charge, and (D) FD electron population.

noticeably affected, thus providing us with information about the internal operation of the cell. The behavior of these cells is currently under investigation.

Acknowledgements—This work was supported by ARPA, NASA, and NSF.

References

[1] C. S. Lent, P. D. Tougaw, W. Porod and G. H. Bernstein, Nanotechnology **4**, 49 (1993).
[2] C. S. Lent, P. D. Tougaw and W. Porod, J. Appl. Phys. **74**, 3558 (1993).
[3] P. D. Tougaw and C. S. Lent, J. Appl. Phys. **75**, 1818 (1994).
[4] T. Fountain, unpublished.
[5] D. V. Averin and K. K. Likharev, in *Mesoscopic Phenomena in Solids* Edited by B. L. Altshuler, P. A. Lee and R. A. Webb, Elsevier, Amsterdam: p. 173 (1991).
[6] M. G. Ancona, J. Appl. Phys. **79**, 526 (1996).
[7] K. Nomoto, R. Ugajin, T. Suzuki and I. Hase, J. Appl. Phys. **79**, 291 (1996).
[8] T. A. Fulton and G. J. Dolan, Phys. Rev. Lett. **59**, 109 (1987).
[9] C. S. Lent and P. D. Tougaw, J. Appl. Phys. **75**, 4077 (1994).
[10] D. Leonard, M. Krishnamurthy, C. M. Reaves, S. P. Denbaars and P. M. Petroff, Appl. Phys. Lett. **63**, 3203 (1993).

[11] M. Field, C. G. Smith, M. Pepper, D. A. Ritchie, J. E. F. Frost, G. Z. C. Jones and D. G. Hasko, Phys. Rev. Lett. **70**, 1311 (1993).
[12] L. W. Molenkamp, K. Flensberg and M. Kemerink, Phys. Rev. Lett. **75**, 4282 (1995).
[13] F. Hofmann, T. Heinzel, D. A. Wharam, J. P. Kotthaus, G. Bohm, W. Klein, G. Trankle and G. Weimann, Phys. Rev. **B 51**, 13872 (1995).
[14] G. L. Snider, M. S. Miller, M. J. Rooks and E. L. Hu, Appl. Phys. Lett. **59**, 2727 (1991).
[15] G. L. Snider, I.-H. Tan and E. L. Hu, J. Appl. Phys. **68**, 5922 (1990).
[16] M. Chen, W. Porod and D. J. Kirkner, J. Appl. Phys. **75**, 2545 (1994).
[17] M. Chen and W. Porod, J. Appl. Phys. **78**, 1050 (1995).
[18] J. H. F. Scott-Thomas, S. B. Field, M. A. Kastner, H. I. Smith and D. A. Antoniadis, Phys. Rev. Lett. **62**, 583 (1990).
[19] A. A. M. Staring, H. van Houten, C. W. J. Beenakker and C. T. Foxon, Phys. Rev. **B 45**, 9222 (1992).
[20] J. Weis, R. J. Haug, K. v. Klitzing and K. Ploog, Phys. Rev. **B 46**, 12837 (1992).
[21] V. Chandrasekhar, Z. Ovadyahu and R. A. Webb, Phys. Rev. Lett. **67**, 2862 (1991).
[22] P. Lafarge, H. Pothier, D. Esteve, C. Urbina and M. H. Devoret, Z. Phys. **B 85**, 327 (1991).